Integral Fast Reactor
Integral Fast Reactor
Integral Fast Reactor
Integral Fast Reactor
Integral Fast Reactor
Integral Fast Reactor
Integral Fast Reactor
Integral Fast Reactor
Integral Fast Reactor
Integral Fast Reactor
Integral Fast Reactor
Integral Fast Reactor
Integral Fast Reactor
Integral Fast Reactor
Integral Fast Reactor
Integral Fast Reactor
Integral Fast Reactor
Integral Fast Reactor
Integral Fast Reactor
Integral Fast Reactor
Integral Fast Reactor
Integral Fast Reactor
Integral Fast Reactor
Integral Fast Reactor
Integral Fast Reactor
Integral Fast Reactor
Integral Fast Reactor
Integral Fast Reactor
Integral Fast Reactor
Integral Fast Reactor
Integral Fast Reactor
Integral Fast Reactor

ANL-IFR-260

An Assessment of the Potential for In-vessel Fission Product Scrubbing Following a Core Damage Event in IFR

by M. T. Farmer
and B. W. Spencer

Argonne National Laboratory, Argonne, Illinois 60439
operated by The University of Chicago
for the United States Department of Energy under Contract W-31-109-Eng-38

~~IFR Technical Memorandum~~
~~Results reported in the IFR-TM series of memoranda frequently are preliminary and subject to revision. Consequently they should not be quoted or referenced.~~

Argonne National Laboratory, with facilities in the states of Illinois and Idaho, is owned by the United States government, and operated by The University of Chicago under the provisions of a contract with the Department of Energy.

March 1995 ANL-IFR-260

AN ASSESSMENT OF THE POTENTIAL FOR IN-VESSEL FISSION PRODUCT SCRUBBING FOLLOWING A CORE DAMAGE EVENT IN IFR

by

M. T. Farmer and B. W. Spencer

Reactor Engineering Division
Argonne National Laboratory
9700 South Cass Avenue
Argonne, IL 60439

IFR TECHNICAL MEMORANDUM NO. 260

~~Results reported in the IFR-TM series of memoranda frequently are preliminary and subject to revision. Consequently they should not be quoted or referenced.~~

TABLE OF CONTENTS

LIST OF FIGURES

LIST OF TABLES

AN ASSESSMENT OF THE POTENTIAL FOR IN-VESSEL FISSION PRODUCT SCRUBBING FOLLOWING A CORE DAMAGE EVENT IN IFR

by

M. T. Farmer and B. W. Spencer

ABSTRACT

A model has been developed to analyze fission product scrubbing in sodium pools. The modeling approach is to apply classical theories of aerosol scrubbing, developed for the case of isolated bubbles rising through water, to the decontamination of gases produced as a result of a postulated core damage event in the liquid metal-cooled IFR. The modeling considers aerosol capture by Brownian diffusion, inertial deposition, and gravitational sedimentation. In addition, the effect of sodium vapor condensation on aerosol scrubbing is treated using both approximate and detailed transient models derived from the literature. The modeling currently does not address thermophoresis or diffusiophoresis scrubbing mechanisms, and is also limited to the scrubbing of discrete aerosol particulate; i.e., the decontamination of volatile gaseous fission products through vapor-phase condensation is not addressed in this study.

The model is applied to IFR through a set of parametric calculations focused on determining key modeling uncertainties and sensitivities. Although the design of IFR is not firmly established, representative parameters for the calculations were selected based on the design of the Large Pool Plant (LPP).

The results of the parametric calculations regarding aerosol scrubbing in sodium for conditions relevant to the LPP during a fuel pin failure incident are summarized as follows. The overall decontamination (DF) for the reference case (8.2 m pool depth, 770 K pool temperature, 2.4 cm initial bubble diameter, 0.1 μm aerosol particle diameter, 1573 K initial gas phase temperature, and 72.9 mole % initial sodium vapor fraction) is predicted to be 36. The overall DF may fall as low as 15 for aerosol particle diameters in the range 0.2-0.3 μm. For particle diameters of <0.06 μm or >1 μm, the overall DF is predicted to be >100. Factors which strongly influence the overall DF include the inlet sodium vapor fraction, inlet gas bubble diameter, and aerosol particle diameter. The sodium pool depth also plays a significant role in determining the overall DF, but the inlet gas phase temperature has a negligible effect on the DF.

I. INTRODUCTION

A. Background

The Integral Fast Reactor (IFR) is an advanced, sodium-cooled fast reactor design with the core region submerged in a large pool of sodium at a pressure slightly above atmospheric. The reference core design uses sodium-bonded metal fuel. The experiments of Planchon et al.[1] have shown that this system is highly tolerant of severe, unprotected transients and is not likely to experience core disruption or fuel melting despite the low melting temperature of the fuel ($T_{solidus}$ = 1423 K).[2] The inherently safe operating characteristics of IFR are principally due to the large thermal conductivity and linear expansion coefficient of the metallic fuel. Nonetheless, it is possible to postulate transients (e.g., unterminated reactivity insertion) that are severe enough that the thresholds for fuel melting and pin failure are surpassed.

The potential implications of fuel pin failure(s) in IFR have been discussed by Spencer and Marchaterre.[3] Specifically, the blowdown of gas and vapor from failed pins into the coolant channels and the resultant expansion process is important to the overall accident sequence from several viewpoints; namely: (i) possible expulsion of the sodium from the fuel assembly, (ii) possible dispersal of molten fuel from the core through drag-related sweepout processes, (iii) possible acceleration of overlying sodium which may impact the vessel head causing damage, and (iv) possible transport of fuel and fission product species to the cover gas region where they may leak from the system. In summary, the pin blowdown and the gas/vapor expansion processes may play varying roles in determining reactivity changes during the accident due to coolant voiding and fuel motion, determining the conversion of expansion energy into mechanical work performed on the reactor head and vessel, and determining the early-time release of radionuclides to the reactor containment. This study addresses the latter of these considerations; i.e., the potential for in-vessel scrubbing of aerosols immediately following a fuel pin failure in IFR. This problem is relevant since any in-vessel scrubbing which occurs during pin failure will mitigate the potential for radionuclide release to the containment should a leak in the primary system develop.

B. Objectives

The main objectives of this study are three-fold:

1. Develop a simplified model for fission product scrubbing in sodium pools using classical theories available in the open literature,

2. apply this model for the conditions relevant to IFR during a postulated core damage event, and

3. assess the potential for early-time, in-vessel retention of fission product radionuclides based on the results of the model application.

A fourth objective of this study is to determine key modeling uncertainties and sensitivities to provide guidance in establishing appropriate conditions for experiments addressing in-vessel fission product scrubbing in IFR.

C. Approach

The modeling approach is to apply classical theories of aerosol scrubbing, developed for the case of isolated bubbles rising through water, to the decon-tamination of gases produced as a result of a core damage event in the liquid metal-cooled IFR. In particular, the modeling considers aerosol capture by Brownian diffusion, inertial deposition, and gravitational sedimentation, as described by Fuchs.[4] These original models, applicable to spherical bubbles,[4] are modified to account for ellipsoidal distortions using the correction factors proposed by Powers.[5,6] In addition, the effect of sodium vapor condensation on aerosol scrubbing is accounted for using a detailed model described herein. However, the model currently does not consider thermophoresis[7] or diffusiophoresis[8] scrubbing mechanisms, and is also limited to the scrubbing of discrete aerosol particulate; i.e., the decontamination of volatile gaseous fission products through vapor-phase condensation is not addressed in this study.

The model is applied through a set of parametric calculations focused on determining key modeling uncertainties and sensitivities. Although the design of IFR is not firmly established, representative parameters for the calculations were selected based on the design of the Large Pool Plant (LPP), which is illustrated in Fig. 1.

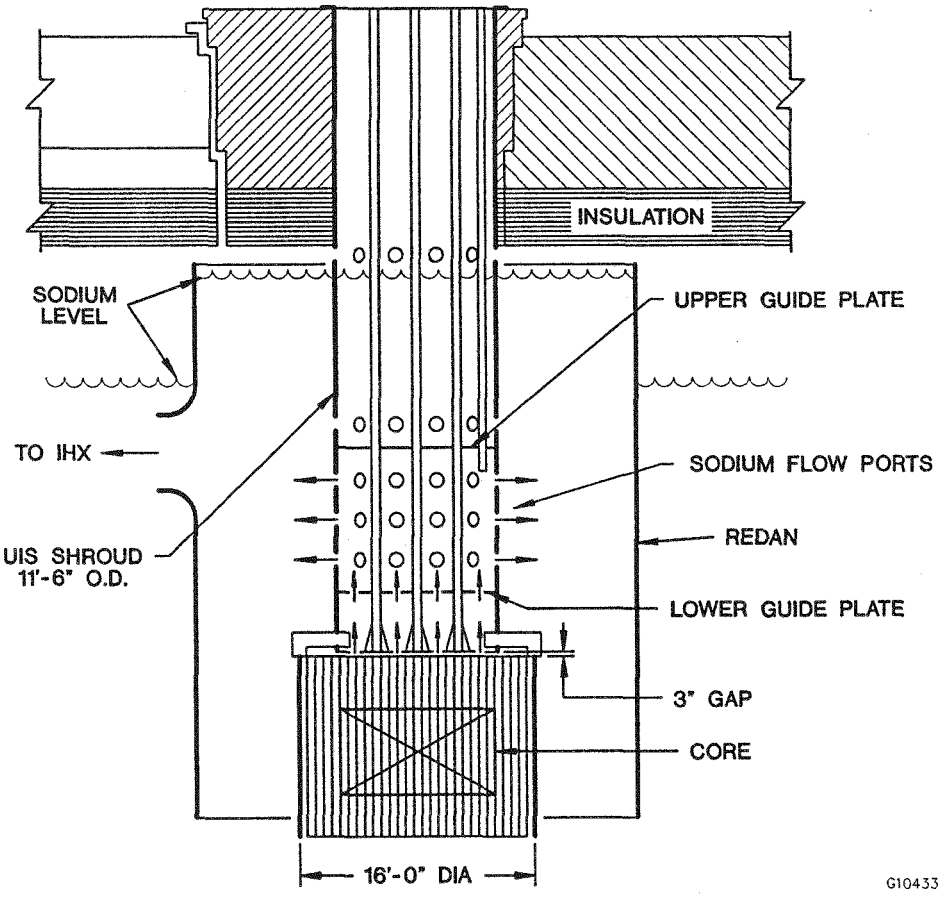

Fig. 1. Elevation View of the Upper Internal Structure of a Large Pool Plant (LPP), a 3500 MWt Sodium-cooled, Pool-type Fast Reactor

D. Related Studies

Fission product scrubbing in water pools has been extensively examined in nuclear reactor safety studies owing to the potential mitigative features attributed to the presence of water in the containment during severe accidents in light water reactors. In particular, for boiling water reactors, the gaseous effluent from the degraded core must pass through a suppression pool designed to

condense steam and retain fission products present in the gas stream. A variety of experiments have been conducted to determine the degree of fission product scrubbing in suppression pools. Much of the early work in this area, which principally focused on quantifying the degree of gaseous iodine retention, has been reviewed by Rastler.[9] More recently, Guntay[10] and Cunnane et al.[11] have conducted experiments which examine the scrubbing of both volatile gases and aerosols. Detailed computer models have also been developed to examine fission product scrubbing in suppression pools. These models include the Suppression Pool Retention Analysis (SUPRA) Code developed by Wassel, Mills, and Bugby,[8] and the Suppression Pool Aerosol Removal Code (SPARC) developed by Owczarski, Schreck, and Postma.[12]

Under the conditions of an ex-vessel severe accident in both boiling and pressurized water reactor containments, it has also been recognized that the presence of water atop a molten core-concrete interaction (MCCI) will scrub fission product aerosols generated as a byproduct of the interaction. This capability has been clearly demonstrated through experiments conducted at both Argonne[13] and Sandia[14] National Laboratories. Computer model development in this area has also been extensive. These models include the VANESA Code developed by Powers, Brockmann, and Shiver[15] in the U.S., and the Bubble Scrubbing Algorithm (BUSCA) developed by Clough, Ramsdale, and Smith[16] in the UK.

Although fission product scrubbing in water pools has been extensively studied, less effort has been devoted to the case when the scrubbing medium is sodium. A limited amount of experiment data is available in the literature addressing fission product retention in sodium. Minges, Schütz, and Seither[17] investigated the transport of volatile gases (elemental iodine and cesium) and UO_2 aerosol through a sodium pool following a high pressure (1 MPa) gas discharge. The experiment was designed to simulate a HCDA in an oxide-fueled LMFBR. The results of their experiments indicate large decontamination factors (DF) of DF $>10^3$ for all fission product simulants with the exception of elemental iodine, for which a DF of 8 was reported. Petrykowski et al.[18] at Oak Ridge National Laboratory investigated the release of UO_2 aerosols from sodium pools. A total of 10 experiments were conducted. The aerosol was generated through capacitor discharge vaporization of UO_2 pellets which were initially submerged in a pool of sodium under an argon covergas.[18] Significant DF's (DF >300) for UO_2 aerosol were reported.

In addition to experimental studies, accidental fission product releases at various fast reactor research facilities have provided valuable data on radionuclide retention in sodium pools. As discussed by Castlemann,[19] the results of the Fermi[20,21] and EBR-II[22-24] incidents indicate substantial release of the various isotopes of the noble gases Xenon and Krypton into the covergas region, while most of the iodine released from the fuel is retained in the liquid sodium.

Analyses which address fission product retention in sodium pools are also limited in the literature. Spencer and Marchaterre[3] performed scoping calculations which indicated that direct contact condensation of sodium vapor as it expands into a sodium pool in a jet mixing regime may occur as rapidly as the vapor emerges from the disrupted core, thereby limiting the ability of an expanding vapor bubble to transport fission product species to the covergas region. Subsequent detailed analyses by Epstein[25] support the potential for large decontamination factors in submerged jets for situations in which the jet injection velocity is at or near the sonic velocity. Jonas and Schütz developed a model to examine scrubbing of aerosols during a HCDA in an oxide-fueled LMFBR. This model treated aerosol scrubbing due to diffusion, inertial deposition, gravitational sedimentation, and absorption by entrained droplets in rapidly expanding and oscillating gas bubbles. The results of their analysis indicate that aerosol particles with a diameter of >2 μm will most likely be absorbed by the liquid due to inertial effects.

II. MODEL DESCRIPTION

A. Summary of Principle Model Assumptions and Limitations

The modeling approach employed in the present study is to utilize classical theories for pool scrubbing[4] which assume that aerosol trapping occurs through particle deposition within isolated bubbles ascending through a liquid pool. Thus, detailed hydrodynamic phenomena such as jet (or plume) flow, bubble agglomeration, bubble shattering, bubble swarms, etc., are not addressed. Detailed models which attempt to incorporate these effects (at least for water pools) are provided elsewhere.[6,8,25] The approach used here is to assume a bubbly flow regime (i.e., isolated bubbles ascending through the pool with a well-characterized terminal rise velocity) where the initial bubble size is limited by hydrodynamic (Taylor[27]) instability.

In terms of the overall accident sequence, the present model addresses fission product scrubbing during the early-time phase of the accident (i.e., a timescale which is not significantly larger than the bubble residence time in the pool). Thus, the model does not address long-term fission product retention in the sodium pool, which is determined by the gas-liquid equilibrium partition coefficients for the volatile fission product species. Studies in this area have been fairly extensive. A general literature review is provided by Castlemann.[19] Equilibrium partition coefficients for cesium, iodine, and tellurium between liquid sodium and the gas phase were recently measured by Haga et al.[28]

The model considers aerosol removal by the mechanisms of Brownian diffusion, inertial deposition, and gravitational sedimentation. In addition, the model accounts for the effects of sodium vapor condensation on aerosol trapping. The model does not treat aerosol removal by the mechanisms of thermophoresis[7] or diffusiophoresis,[8] nor does the model address the effects of particle growth by coagulation and/or sorption on the overall aerosol removal rate. Finally, the model is currently limited to the treatment of discrete aerosol particulate; i.e., the decontamination of volatile gaseous fission products via vapor-phase condensation is not addressed.

B. Aerosol Transport Equations

The principal objective of the analysis is to calculate the pool decontamination factor, DF, which is defined as the ratio of the aerosol mass entering the pool to the aerosol mass exiting the pool, i.e.,

$$DF = \frac{\text{Aerosol mass entering the sodium pool}}{\text{Aerosol mass exiting the sodium pool}}. \qquad (1)$$

As summarized above, the current study addresses aerosol removal by the mechanisms of Brownian diffusion, inertial deposition, gravitational sedimentation, and vapor condensation. For a given aerosol particle diameter, d_a, the differential equation governing the rate of aerosol removal from the bubble for the j-th removal mechanism is of the form,

$$\left(\frac{dn}{dz}\right)_j = - \alpha_j \, n \qquad (2)$$

where

n = number of particles in the bubble with diameter d_a,

z = coordinate parallel to the direction of the bubble flux, and

α_j = removal rate coefficient for the j-th scrubbing mechanism (diffusion, inertia, sedimentation, condensation).

For the purposes of this study, the various removal mechanisms are treated as independent. Under this assumption, the total particle removal rate is calculated as the sum of the removal rates for the individual mechanisms, i.e.,

$$\frac{dn}{dz} = - \sum_j \alpha_j \, n. \qquad (3)$$

As discussed by Webb,[29] the assumption of the independent removal mechanisms is valid for spherical bubbles, but can lead to a significant underprediction of the aerosol removal rate for highly deformed (ellipsoidal) bubbles when the vapor condensation rate is high. However, a more general treatment to account for this effect is beyond the current scope of work.

Integration of Eq. (3) over the pool depth yields the number of aerosol particles with a given diameter exiting the pool upper surface. With this result, the DF for the given particle size is then evaluated through Eq. (1).

C. Aerosol Removal Rate Constants

The rate constants in Eqs. (2) and (3) for aerosol removal by diffusion, inertia, sedimentation, and condensation scrubbing mechanisms are defined in this section.

1. Brownian Diffusion

The rate constant for aerosol scrubbing by Brownian diffusion, as corrected by Powers[6] for the case of ellipsoidal bubble deformations, is of the form:

$$\alpha_D = 6\sqrt{\frac{8\theta}{\pi U_B D_B^3}}\left[\frac{(E^2 - 1)\,F(E)}{1 + \sqrt{4 + 2(E^2 - 1)}}\right], \tag{4}$$

where

$$\theta = \frac{K T_B C}{3 \pi \mu_g d_a}, \tag{5}$$

T_B = bubble bulk gas temperature (absolute),

U_B = bubble rise velocity,

D_B = average bubble diameter,

K = Boltzman constant = $1.3807 \cdot 10^{-23}$ J/K,

C = Cunningham slip correction,

$$C = 1 + \left(\frac{2\lambda}{d_a}\right)\left[1.257 + 0.4 \exp\left(-0.55\, d_a/\lambda\right)\right], \tag{6}$$

λ = mean free path of gas molecule,

$$\lambda = \frac{K T_B}{\sqrt{2}\,\pi\, d_g^2\, P_B}, \tag{7}$$

d_a = aerosol particle diameter,

d_g = effective gas molecule diameter,

P_B = bubble absolute pressure,

μ_g = gas viscosity,

E = bubble eccentricity, and

$$F(E) = \left[\frac{1.76\ E^2}{E^2 - 1} - \sqrt{2}\right]^{1/2} \left[\frac{E^2 \tan^{-1}\left(\sqrt{E^2 - 1}\right)}{\sqrt{E^2 - 1}} - 1\right]^{-1/2}. \quad (8)$$

The eccentricity is defined as the ratio of the lengths of the major and minor axes of the bubble. For a spherical bubble, the eccentricity is therefore equal to 1. Correlations for the bubble eccentricity and rise velocity are provided later in this section. In the limit as $E \rightarrow 1$, Eq. (4) reduces to,[6]

$$\alpha_D = 1.83 \sqrt{\frac{8\theta}{\pi\ U_B\ D_B^3}}. \quad (9)$$

Note that the diffusion rate constant decreases as either the aerosol particle diameter or the gas bubble diameter decreases.

2. Inertial Deposition

The rate constant for aerosol scrubbing by inertial deposition, including the effect of ellipsoidal bubble deformations,[6] is of the form:

$$\alpha_I = \frac{6\ U_B\ \tau\ G(E)}{D_B^2}, \quad (10)$$

where

$$\tau = \frac{\rho_a\ d_a^2\ C}{18\ \mu_g}, \quad (11)$$

$$G(E) = \frac{E^{4/3}\left[(E^2 - 1)^2 + (E^2 - 1)^{3/2}(E^2 - 2)\tan^{-1}\left(\sqrt{E^2 - 1}\right)\right]}{\left[\sqrt{E^2 - 1} - E^2 \tan^{-1}\left(\sqrt{E^2 - 1}\right)\right]^2}. \quad (12)$$

In the limit as E → 1, Eq. (10) reduces to,[6]

$$\alpha_I = \frac{18\, U_B\, \tau}{D_B^2}. \qquad (13)$$

Note that the inertial deposition rate constant increases with increasing aerosol particle diameter, and decreases with increasing gas bubble diameter.

3. Gravitational Sedimentation

The rate constant for gravitational sedimentation, modified for ellipsoidal bubble deformations,[6] is of the form:

$$\alpha_S = \frac{1.5\, g\, \tau\, E^{2/3}}{D_B\, U_B}, \qquad (14)$$

where g = gravitational acceleration. The sedimentation rate constant for the case of a spherical bubble is obtained by setting E = 1 in the above equation. From Eqs. (11) and (14), note that the sedimentation scrubbing rate increases with increasing aerosol particle diameter, and decreases with the average gas bubble diameter.

4. Condensation

The rate constant for aerosol scrubbing by vapor condensation at the gas/liquid interface is given through the expression,[8]

$$\alpha_c = \frac{-\,6\, \dot{m}_v}{A_B\, D_B\, U_B\, \rho_g}, \qquad (15)$$

where

$\dot{m}_v$ = steam generation rate at the gas/liquid interface,
A_B = bubble surface area = $\pi\, D_B^2$, and

ρ_g = bubble gas density.

The steam generation rate, $\dot{m}_v$, is taken to be positive if vaporization is occurring at the interface. As is evident from Eqs. (3) and (15), vapor condensation $\left(\dot{m}_v < 0\right)$ acts to augment aerosol scrubbing. Conversely, the vapor flux from the interface during vaporization $\left(\dot{m}_v > 0\right)$ acts to suppress scrubbing. Note that no attempt has been made here to account for the effects of bubble deformation (eccentricity) on the condensation scrubbing rate. The assumption that the condensation scrubbing rate is independent of bubble shape should be valid as long as surface characteristics (i.e., curvature) do not significantly affect the local interfacial mass and energy balances governing the condensation rate. The modeling approach for evaluating the condensation rate is described below.

D. Bubble Conservation Equations

The principal objective of the modeling described in this section is to evaluate the vapor condensation rate at the bubble surface. This information is then used to calculate the condensation rate constant for aerosol scrubbing, defined in Eq. (15). The condensation rate is determined by solving a coupled set of equations governing mass and energy transfer at the bubble gas/liquid interface.

Sherwood and Pigford[30] provide the following expression for the vapor flux across a phase change interface:

$$\dot{m}_v'' = - M_v \, k_v^* \, \ln\left(\frac{1 - X_v^i}{1 - X_v}\right) \tag{16}$$

where

$$\dot{m}_v'' = \frac{\dot{m}_v}{A_B}, \tag{17}$$

M_V = molecular weight of vapor,

k_v^* = interfacial mass transfer coefficient (moles/m^2·s),
X_v = mole fraction vapor in the bubble bulk gas mixture, and
X_v^i = mole fraction vapor at the interface.

As is evident from the above expression, the simplifying assumption has been made that transient effects insofar as determining the mass transfer rate at the interface are negligible, and therefore the equation for the mass flux is written in quasi-steady form. An expression for the interfacial mass transfer coefficient, k_v^*, is provided at the end of this section.

The mole fraction of vapor in the gas mixture at the interface, X_v^i, is related to the bubble internal pressure and the vapor partial pressure through the expression:

$$X_v^i = \frac{P_v\left(T_i\right)}{P_B} \tag{18}$$

where

T_i = bubble gas/liquid interfacial temperature, and
$P_v\left(T_i\right)$ = vapor partial pressure evaluated at the interface temperature, T_i.

The bubble internal pressure is assumed to equal the local hydrostatic pressure at the given bubble submergence depth, i.e.,

$$P_B = P_{sys} + \rho_l\, g\, z_D \tag{19}$$

where

P_{sys} = system pressure,
ρ_l = coolant density,
g = gravitational acceleration, and
z_D = bubble submergence depth.

Note that the above relationship is based on the assumption that the effect of surface tension (curvature) on the bubble pressure is negligible. Given the current bulk gas temperature and

pressure, the bubble volume is then evaluated through the ideal gas law, which takes the following form for a mixture of gases:

$$P_B = \frac{R_g T_B}{V_B} \sum_k \frac{m_k}{M_K}, \tag{20}$$

where

R_g = universal gas constant = $8314 \ \frac{J}{mole \cdot K}$,

$$V_B = \text{bubble volume} = \frac{\pi D_B^3}{6}, \tag{21}$$

m_k = mass of k-th constituent in the gas phase, and

M_k = molecular weight of k-th gas constituent.

To complete the model for evaluating the vapor generation rate at the bubble surface, a second relationship is required which relates $\dot{m}_v$ to the interface temperature, T_i. The expression is provided by applying conservation of energy at gas/liquid interface, which yields

$$e_{lv} \dot{m}_v = A_B \left(h_P \left(T_P - T_i \right) - h_g \left(T_i - T_B \right) \right) \tag{22}$$

where

T_P = pool temperature,

h_P = convective heat transfer coefficient from the pool to the bubble surface,

h_g = convective heat transfer coefficient from the bulk gas to the bubble surface, and

e_{lv} = coolant latent heat of vaporization.

Expressions for the convective heat transfer coefficients, h_P and h_g, are provided at the end of this section. The coolant temperature in the above equation is assumed to remain constant over the bubble passage time through the pool. At a given time, the vapor generation rate, $\dot{m}_v$, is found by first combining Eqs. (16), (17), and (22) to obtain a single transcendental equation for the bubble

surface temperature, T_i. This transcendental equation, in conjunction with the thermodynamic constraint defined by Eq. (18), is solved for T_i using a Newton-Raphson iterative technique (e.g., see Kreyzig[31]). Given T_i and the current bubble gas temperature, T_B, the vapor generation rate is then evaluated directly from Eq. (22).

With the above methodology for evaluating the vapor generation rate, a final equation is required for the bubble bulk gas temperature, T_B. Following the approach of Clough et al.[16] the conservation of energy equation for the bubble gas temperature is of the form:

$$\frac{dT_B}{dt} = \frac{1}{m_g C_g} \left\{ - h_g A_B \left(T_B - T_i\right) + \left[e_v \left(T_i\right) - e_V \left(T_B\right)\right] \dot{m}_v \right\} \tag{23}$$

where

m_g = total bubble gas mass,

c_g = gas specific heat, and

$e_v (T_i)$, $e_v (T_B)$ = coolant vapor specific enthalpy evaluated at the bubble interface and bulk gas temperatures, respectively.

The above equation is expressed in terms of a Lagrangian coordinate system, while the aerosol removal rate equations [Eqs. (2) and (3)] are expressed in terms of Eulerian coordinates. Equation (23) can be rewritten in an Eulerian framework through the following change of coordinates:

$$\frac{dT_B}{dx} = \frac{dT_B}{dx} \frac{dx}{dt} = U_B \frac{dT_B}{dx}, \tag{24}$$

which yields,

$$\frac{dT_B}{dx} = \frac{1}{m_g C_g U_B} \left\{ - h_g A_B \left(T_B - T_i\right) + \left[e_v \left(T_i\right) - e_v \left(T_B\right)\right] \dot{m}_v \right\}. \tag{25}$$

For a given aerosol particle diameter, the above expression is simultaneously integrated over the depth of the pool with the aerosol removal rate equations [Eqs. (2) and (3)], in conjunction with

the auxiliary expressions for the rate constants [Eqs. (4), (10), (14), and (15)], bubble pressure and volume [Eqs. (19) and (21)], and vapor condensation rate [Eqs. (16) and (19) and (22)], to obtain the aerosol particle mass exiting the pool upper surface. The decontamination factor (DF) for the given particle diameter is then evaluated through Eq. (2). The integration is performed using a standard fourth-order Runge-Kutta (Gill) method; the subroutine is taken directly from White.[32]

E. Model Simplifications

As described in the previous section, a numerical algorithm is required to solve the simultaneous set of equations governing aerosol transport through the sodium pool. The principal reason why a numerical solution is required is that the auxiliary equations governing the vapor condensation rate are highly non-linear. As an alternative approach, a simplified model for aerosol scrubbing due to vapor condensation is provided below. With the condensation problem simplified, a numerical solution is no longer required to obtain approximate estimates of aerosol scrubbing in sodium including the effects of vapor condensation.

The following model for estimating the effect of vapor condensation on aerosol scrubbing was developed by Owcsarski et al.[12] The basic assumptions underlying the model are: (i) the gas within the bubble attains thermal equilibrium with the pool in the immediate vicinity of the bubble entry point, and (ii) the aerosol particles are swept along with the condensing vapor, so that the fraction of particles captured due to condensation is directly proportional to the fraction of gas that condenses. Given the first assumption, the initial condition on the bubble gas temperature becomes:

$$T_B = T_P. \tag{26}$$

Given the second assumption, a condensation DF can be derived based on the fraction of inlet gas condensed, i.e.,[12]

$$DF_c = \frac{1}{1 - F} = \frac{X_{nc}^{eq}}{X_{nc}^{i}}, \tag{27}$$

where

F = volume (mole) fraction inlet gas condensed,

X_{nc}^{eq} = mole fraction noncondensables in bubble after thermal equilibrium is attained, and

X_{nc}^{i} = mole fraction noncondensables in the inlet gas.

Note that Eq. (27) is independent of aerosol particle size.

If the additional assumption is made that the variation of hydrostatic pressure with submergence depth does not significantly affect the rate constants for diffusion, inertial deposition, and sedimentation removal processes, then simplified solutions may be obtained for these processes also. Under the assumption that the rate constants do not vary with submergence depth, then integration of Eq. (2) subject to the initial condition $n\ (z = o) = n_o$ yields,

$$n = n_o\, e^{-\alpha_j z} \tag{28}$$

where

n_o = number of aerosol particles in the bubble with diameter d_a at the injection point, and subscript j denotes diffusion, inertial deposition, and sedimentation scrubbing processes. For a given aerosol particle diameter, d_a, DF's for the individual scrubbing processes are then found from Eqs. (1) and (28) as,

$$DF_D = e^{\alpha_D H_P}, \tag{29}$$

$$DF_I = e^{\alpha_I H_P}, \tag{30}$$

$$DF_s = e^{\alpha_S H_P}, \tag{31}$$

where

H_P = initial bubble submergence depth.

Note that the hydrostatic (i.e., bubble) pressure has been evaluated at the initial bubble submergence depth for the purposes of evaluating the rate constants in Eqs. (29) through (31). For a given particle diameter, a cumulative DF for all scrubbing processes is then found by combining Eqs. (27) and (29) through (31), which yields

$$DF = \frac{X_{nc}^{eq}}{X_{nc}^{i}} e^{(\alpha_D + \alpha_I + \alpha_S)} \tag{32}$$

or

$$DF = DF_C \, DF_I \, DF_D \, DF_S. \tag{33}$$

Note carefully that when condensation is included in the model, the rate constants for diffusion, inertia, and sedimentation scrubbing processes are evaluated based on the bubble diameter after vapor condensation has occurred (i.e., the bubble has thermally equilibrated with the surrounding coolant).

F. Auxiliary Relationships

Correlations for initial bubble volume, bubble rise velocity, bubble eccentricity, and bubble convective heat and mass transfer coefficients are provided in this section.

1. Initial Bubble Volume

A detailed analysis of the mechanisms leading to bubble formation during fuel pin failure in IFR is beyond the current scope of work. Rather, the assumption is made that the initial bubble size is limited by hydrodynamic (i.e., Taylor[27]) instability as gases and aerosols from failed fuel pin(s) exit the top of the fuel assembly into the overlying coolant pool. Thus, the initial bubble diameter is given through the expression

$$D_B = \frac{\lambda}{2} \tag{34}$$

where

λ = Taylor wavelength[27]

$$= 2\Pi \sqrt{\frac{3\,\sigma_l}{g\left(\rho_l - \rho_g\right)}}, \tag{35}$$

σ_l = coolant surface tension.

Variations in bubble diameter from that predicted by Eq. (34) are addressed through parametric calculations which are described in the next section. Given the initial bubble diameter through Eq. (34), the corresponding bubble volume is evaluated through Eq. (21).

2. Bubble Rise Velocity

The bubble rise velocity is estimated using the correlation of Peebles and Garber,[33] which was developed on the basis of gas bubbles rising in water,

$$U_B = \begin{cases} \dfrac{2\,R_b^2\left(\rho_l - \rho_g\right)g}{9\,\mu_l}; & Re_B < 2, \\ 0.33\,g^{0.76}\left(\dfrac{\rho_l}{\mu_l}\right)^{0.52} R_B^{1.28}; & 2 \le Re_B < 4.02\,M_o^{-0.214}, \\ 1.35\left(\dfrac{\sigma_l}{\rho_l R_B}\right)^{0.5}; & 4.02\,M_o^{-0.214} \le Re_B < 3.10\,M_o^{-0.15}, \\ 1.18\left(\dfrac{g\,\sigma_l}{\rho_l}\right)^{0.25}; & 3.10\,M_o^{-0.125} \le Re_B, \end{cases} \tag{36}$$

where

μ_l = coolant viscosity,

$R_B = \frac{D_B}{2}$,

Re_B = bubble Reynolds number,

$$Re_B = \frac{\rho_l R_B U_B}{\mu_l}, \tag{37}$$

M_o = Morton number, and

$$M_o = \frac{g \mu_l^4}{\rho_l \sigma_l^3}. \tag{38}$$

3. Bubble Eccentricity

As discussed earlier, the bubble eccentricity is defined as the ratio of the major and minor axes of the bubble. The eccentricity is estimated using the correlation recommended by Powers,[6] which was developed on the basis of gas bubbles rising in water,

$$\frac{1}{E} = \begin{cases} 1; \ Ta \le 1, \\ \{0.81 + 0.206 \tanh [2(0.8 - \log_{10} Ta)]\}^3 \\ 0.24; \ Ta > 39.8, \end{cases} \tag{39}$$

where

Ta = Tadaki number = $\hat{Re}_B Mo^{0.23}$, (40)

and, in this application,

$$\hat{Re}_B = \frac{\rho_l D_B U_B}{\mu_l} \tag{41}$$

4. Bubble Heat and Mass Transfer Coefficients

The convective heat transfer coefficients in Eq. (22) are evaluated using the same correlations adopted by Wassel et al.[18] for use in the SUPRA fission product scrubbing code (developed for LWR's). Inside the bubble, a Hill's vortex circulation pattern is assumed. In this case, the Nusselt number governing the convective heat transfer from the gas phase to the bubble surface is given through the expression developed by Kronig and Brink,[34] i.e.,

$$Nu_g = \frac{h_g D_B}{k_g} = 17.9 \tag{42}$$

where

k_g = gas phase thermal conductivity.

The convective heat transfer coefficient on the liquid side of the interface is evaluated using the methodology proposed by Huang and McDonald,[35] viz.,

$$Nu_l = \left(\frac{D_B}{\sqrt{\pi \alpha_l t}}, 2.0 + 0.6 \left(\hat{Re}_B\right)^{1/2} Pr_l^{1/3} \right) \tag{43}$$

where

$$Nu_l = \frac{h_P D_B}{k_l}, \tag{44}$$

$$Pr_l = \frac{\nu_l C_l}{k_l}, \tag{45}$$

$$\alpha_l = \frac{k_l}{\rho_l C_l}, \tag{46}$$

k_l, C_l = coolant thermal conductivity and specific heat, respectively,

and the operator $\langle \cdot, \cdot \rangle$ in Eq. (43) denotes the larger of the two arguments.

The mass transfer coefficient in Eq. (16) is evaluated using the following correlation recommended by Sherwood, Pigford, and Wilke,[30]

$$k_v^* = \frac{h_g}{C_g \overline{M}_g} \left(\frac{Pr_g^{2/3} \beta}{Sc_g^{2/3}} \right) \tag{47}$$

where

Sc_g = Schmidt number for gas phase,

$$= \frac{\mu_g}{\rho_g D_{vg}}, \tag{48}$$

D_{vg} = mass transfer coefficient between the vapor and noncondensable gas species,

$$Pr_g = \frac{\mu_g C_g}{k_g},$$

$\overline{M}_g$ = average molecular weight of gas,

and β is a dimensionless correction to the mass transfer coefficient for situations in which the mass

transfer rate is high,[30]

$$\beta = \frac{\overline{M}_i \ln\left(\overline{M}_i/\overline{M}_g\right)}{\left(\overline{M}_v - \overline{M}_{NC}\right)\left(1 - X_v^i\right)\ln\left(\frac{1 - X_v}{1 - X_v^i}\right)}, \tag{49}$$

where

$\overline{M}_i$ = average molecular weight of gas at vaporization/condensation interface,

$\overline{M}_g$ = average molecular weight of bubble bulk gas, and

$\overline{M}_{nc}$ = average molecular weight of noncondensables (excluding vapor).

The mass transfer coefficient in Eq. (48) is evaluated using the following expression recommended by Bird, Stewart, and Lightfoot,[36] which is applicable to a mixture of gases:

$$D_{vg} = \frac{1 - X_v}{\sum_k X_k/D_{vk}} \tag{50}$$

where

X_k = mole fraction k-th constituent in gas phase, and

D_{kv} = binary diffusion coefficient between coolant vapor and the k-th gas constituent.

Note that the sum on k in the denominator of Eq. (50) does not include the vapor constituent. The binary diffusion coefficients, D_{vk}, are calculated with the following correlation[37]

$$D_{vk} = \frac{a}{P_B}\left(\frac{T_B}{\sqrt{T_c^k\, T_c^v}}\right)^b \left(\frac{1}{M_v} + \frac{1}{M_k}\right)^{1/2} \left(T_c^k\, T_c^v\right)^{5/12} \left(P_c^k\, P_c^v\right)^{1/3} \tag{51}$$

where subscript c denotes a critical property, and the constants a and b are empirical constants which are defined as follows:

For nonpolar gas pairs: $a = 4.047 \cdot 10^{-8}$, $b = 1.823$

For H_2O with a nonpolar gas: $a = 5.366 \cdot 10^{-8}$, $b = 2.334$

Note that Eq. (51) is not dimensionless. The empirical constants a and b are specified such that all variables in Eq. (51) are SI units (i.e., $[D_{vk}] = m^2/s$, [P] = Pa, [T] = K, and [M] = kg/mole).

III. MODEL VALIDATION

To date, only a very limited set of validation calculations have been performed with the fission product scrubbing model described in this study. The principal reason for this is the lack of experiment data available in the literature regarding aerosol trapping in sodium under conditions applicable to IFR. The experiments which have been conducted[17,18] have addressed fission product scrubbing following a high pressure gas discharge under sodium (i.e., simulations of a HCDA in an oxide-fueled LMFBR). As described in Sect. I, this is not expected to be a viable accident sequence for IFR owing to the inherent safety characteristics associated with this reactor.[1]

The single validation calculation which has been performed includes a comparison of the model with the vapor bubble collapse data obtained by Florschuetz and Chao[38] in a water pool (note that the authors are not aware of analogous data obtained in sodium). In these experiments, saturated steam bubbles containing noncondensable gas were subject to a step increase in pool pressure. The bubble radius as a function of time was then measured as the bubbles collapsed. Note that the tests were conducted under free fall conditions such that the bubble translation velocity in the pool was essentially zero, and therefore the bubbles underwent nearly symmetrical collapse.[38]

The particular experiment selected for analysis in Ref. 38 was Test No. 1WX. This test was chosen since the noncondensable gas initially present in the bubble was Xenon, which is the

dominant fission product species expected to be present in the fuel at the time of pin failure in IFR.[3] The assumed conditions for the experiment are shown in Table I. The initial bubble diameter, D_B, was set equal to the reported value in Ref. 38, as opposed to the diameter which would be expected on the basis of hydrodynamic instability [see Eq. (34)]. Since the experiments were conducted with essentially zero translation velocity, the convective heat transfer coefficient on the pool side of the bubble gas/liquid interface was evaluated with the transient expression defined in Eq. (46), which is applicable in situations where no convection is present.

TABLE I. Experiment Conditions for Test No. 1WX of Florschuetz and Chao [38]

Parameter	Variable Name	Value
Initial System Pressure (kPa)	-----	67.0
Initial Coolant Temperature (K)	T_P	362.0
System Pressure After Step Increase (kPa)	P_{sys}	98.7
Initial Bubble Diameter (mm)	D_B	7.52
Initial Mole Fraction Steam in Bubble (--)	X_v^i	0.916
Initial Mole Fraction Gas in Bubble (--)*	X_{nc}^i	0.084

*Reported as 0.066 in Ref. 38 plus a small (but unspecified) amount of air. The value shown in the table has been increased slightly to account for the presence of the air.

The calculated bubble radius as a function of time after the step increase in pressure for Test No. 1WX is shown in Fig. 2. The experiment data[38] is also shown in the figure. Note that the initial (t = 0) step change in bubble radius predicted by the model reflects the (adiabatic) equilibration of the bubble to the higher pressure level according to the ideal gas law [see Eq. (20)].

During this initial phase, the bubble collapse is actually governed by the inertia of the coolant, which has not been accounted for in the current model (i.e., an explicit momentum equation governing the bubble radius as a function of time has not been solved). The reader is referred to the study by Forster and Zuber,[39] in which the effects of coolant inertia on bubble collapse have been considered. The inertially controlled collapse phase is, however, quite short.[39] Thereafter, the bubble collapse is controlled by heat transfer at the gas/liquid interface. As is evident from Fig. 2, the model shows reasonable agreement with the experiment data during this phase.

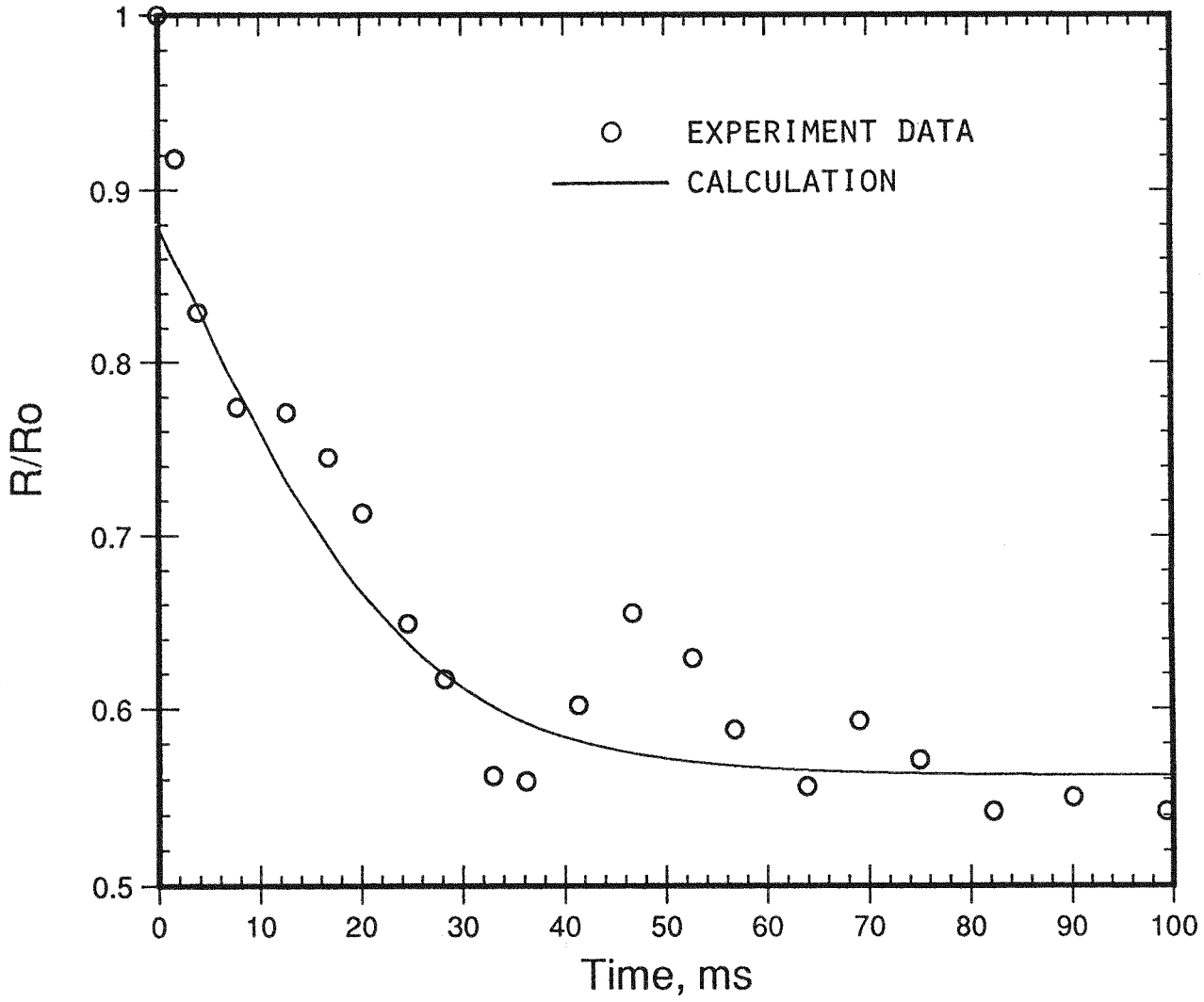

Fig. 2. Comparison of Model Predictions with the Experiment Data of Florschuetz and Chao[38] for the Condensation of a Steam Bubble Containing Noncondensable Xenon Gas.

IV. MODEL APPLICATION TO IFR

Although the design of IFR is not firmly established, representative parameters for the analysis were selected based on the design of the Large Pool Plant (LPP), which is illustrated in Fig. 1. The present model has been applied to this design through a set of parametric calculations focused on determining key modeling uncertainties and sensitivities regarding the potential for in-vessel aerosol retention following fuel pin failure(s) in IFR. The technical basis for selecting the various input parameters is provided first, followed by the presentation of the results of the parametric calculations. The study is then concluded with a general discussion regarding the results of the calculations.

A. Input Parameter Selection

The principal physical parameters which affect aerosol scrubbing according to the present model are summarized in Table II. Overall system parameters include the pool depth, temperature, and plenum pressure. Other key variables include the inlet gas bubble diameter and the aerosol particle diameter. Aerosol attenuation is also dependent upon the inlet gas vapor fraction, inlet pressure, and inlet gas temperature. However, as will be illustrated in the calculations which follow, scrubbing in sodium is only weakly affected by variations in inlet gas temperature and pressure, since the bubbles are predicted to undergo rapid thermal equilibration within a distance of a few bubble diameters from the injection point into the pool.

The total estimated core-wide inventories of gaseous and volatile fission product species, including sodium contained in the fuel porosity, is shown in Table III.[3] The normal boiling temperatures for the various species are also shown in the table. The table conservatively assumes that the fission products are present in their elemental form. However, recent studies[28] indicate that most of the Iodine will probably be present in the form of CsI. For the purposes of the current work, the aerosol particles are therefore assumed to consist of CsI, since the vapor pressure of this compound is low at the sodium boiling temperature of 1156 K (the normal boiling temperature of CsI is 1553 K). The aerosol particle density is thus taken equal to 4510 kg/m^3, which is the reported value for CsI.[40] The nominal aerosol particle diameter is taken equal to 0.1 μm. The parametric

TABLE II. Reference Conditions and Parameter Ranges for Parametric Calculations

Variable	Symbol	Reference Value	Range	Units
Pool depth	H_p	8.2	0-10	m
Pool temperature	T_p	770	770-970	K
Plenum pressure	P_{sys}	0.1	-----	MPa
Inlet gas temperature	T_i	1570	-----	K
Inlet gas pressure	P_i	0.2	-----	MPa
Inlet gas vapor content	X_v^i	72.9	1-99	mole %
Inlet bubble diameter	D_b	2.4	0.1-10	cm
Aerosol particle density	ρ_a	4510*	-----	kg/m^3
Aerosol particle diameter	d_a	0.1	0.01-10	μm

*Assumed to equal the density of CsI.[40]

TABLE III. Assumed Inventory of Gaseous and Volatile Species in LPP Metal Fuel after 1-year Full Power Operation at 3500 MWt from Ref. 3. The normal boiling temperatures are taken from Ref. [40].

Species[a]	Inventory, moles	mole %	Normal Boiling Temperature, K
Xe	1490	13.7	165
Kr	220	2.0	120
I	70	0.6	457
Rb	90	0.8	961
Cs	930	8.6	944
Te	150	1.4	1261
Bond Na[b]	7910	72.9	1156

[a]Trace amount of Br and Se neglected.

[b]Contained in fuel porosity.

calculations consider particle diameters ranging from 0.01-10 μm. The balance of the fission product species (i.e., Xe, Kr, Rb, and Cs not bound as CsI) are assumed to be present in gaseous form.

The sodium pool depth is nominally set equal to 8.2 m, which is the approximate distance from the top of the fuel assemblies to the upper surface of the sodium adjacent to the covergas region in the reference LPP design shown in Fig. 1. The system operating pressure is assumed to equal atmospheric pressure (0.1 MPa). The normal hot pool operating temperature is ~770 K[3] for the LPP design; the largest credible increase in coolant temperature due to a postulated overpower accident is ~200 K[3] owing to the large heat sink offered by the sodium pool. Thus, parametric calculations have been performed over the coolant temperature range of 770-970 K.

The inlet gas bubble temperature and pressure are based on the analyses of Spencer and Marchaterre,[3] who considered the two-phase axial blowdown of a fuel subassembly following a fuel pin failure. The results of their scoping analyses indicate that the gas temperature and pressure at the exit of the top of the fuel assemblies will be ~1570 K and ~0.2 MPa, respectively. These are the assumed inlet conditions for the calculations. However, as discussed previously, the aerosol scrubbing results are relatively insensitive to these input parameters, since the gas bubbles rapidly reach thermal equilibrium with the surrounding coolant. The inlet gas vapor fraction is nominally taken equal to the value shown in Table III, which is 72.9 mole %. The parametric calculations consider sodium vapor contents of 1-99 mole %. The nominal inlet gas bubble diameter at the top of the subassemblies is set equal to 2.4 cm, which is the expected value assuming that the initial bubble size is limited by Taylor instability[27] (see Eq. (34)); the assumed sodium coolant density and surface tension are 830 kg/m^3 and 0.16 N/m, respectively[41]). The calculations consider inlet bubble diameters ranging from 0.1-10 cm.

Aside from the physical parameters discussed above, the aerosol scrubbing model is dependent upon the thermophysical properties of the coolant, the coolant vapor, and the fission product gases present in the bubble. The coolant and coolant vapor properties were taken from Ref. 41, while the thermophysical properties for the fission product gases were predominantly taken from Ref. 40.

B. Results and Discussion

The aerosol DF's for diffusion, inertial deposition, sedimentation, and condensation scrubbing mechanisms are shown in Fig. 3 versus bubble rise distance in the pool for the reference case (see Table II). These solutions were generated by numerical integration of the detailed aerosol transport equations de-fined in Eqs. (2) and (3), along with the auxiliary expressions for the aerosol scrubbing rate constants defined in Eqs. (4), (10), (14), and (15). As is evident from this figure, condensation scrubbing occurs over a very short bubble rise distance, owing to the rapid thermal equilibration of the bubble with the surrounding coolant. This effect is shown in greater detail in Figs. 4 and 5, where the bubble radius, bulk gas temperature, sodium vapor fraction, and aerosol DF's for the various scrubbing mechanisms have been plotted over the first 20 cm of bubble travel. Note from Fig. 4 that the bubble has essentially reached thermal equilibrium with the surrounding coolant after traveling ~10 cm, which corresponds to ~4 bubble diameters based on the initial bubble size (2.4 cm). Thereafter, aerosol removal by condensation is essentially negligible, and the other scrubbing mechanisms begin to dominate as the bubble ascends through the balance of the pool. The overall DF for the reference case conditions is noted to be 36 from Fig. 3.

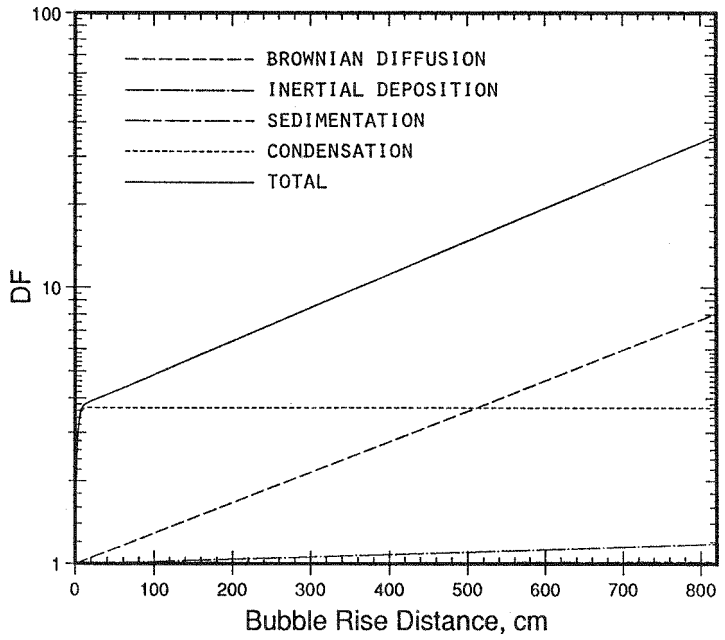

Fig. 3. DF's for the Different Scrubbing Mechanisms Considered in the Current Analysis Versus Bubble Rise Distance for the Reference Case (see Table II).

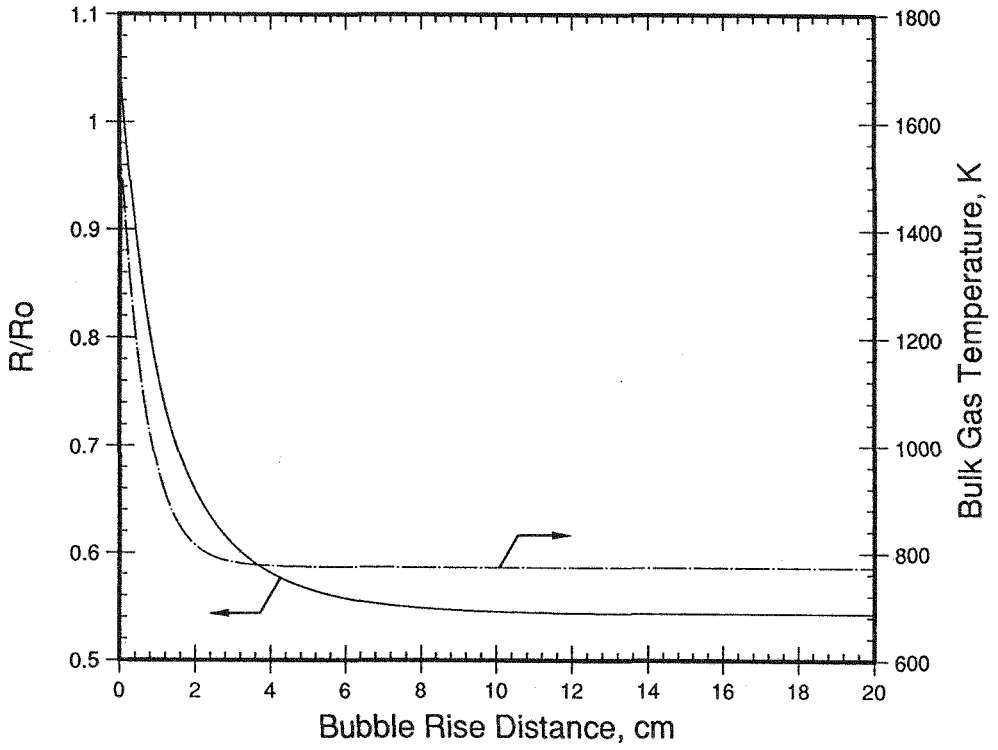

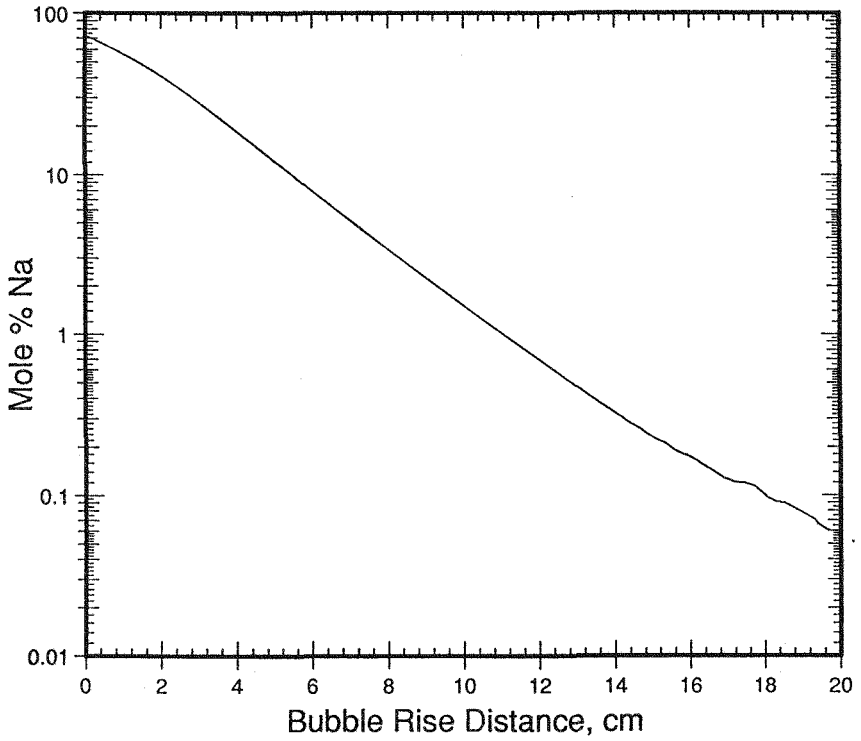

Fig. 4. Calculated Bubble Radius, Bulk Gas Temperature, and Sodium Vapor Content Versus Bubble Rise Distance in the Pool for the Reference Case (see Table II). The initial bubble radius is 1.2 cm.

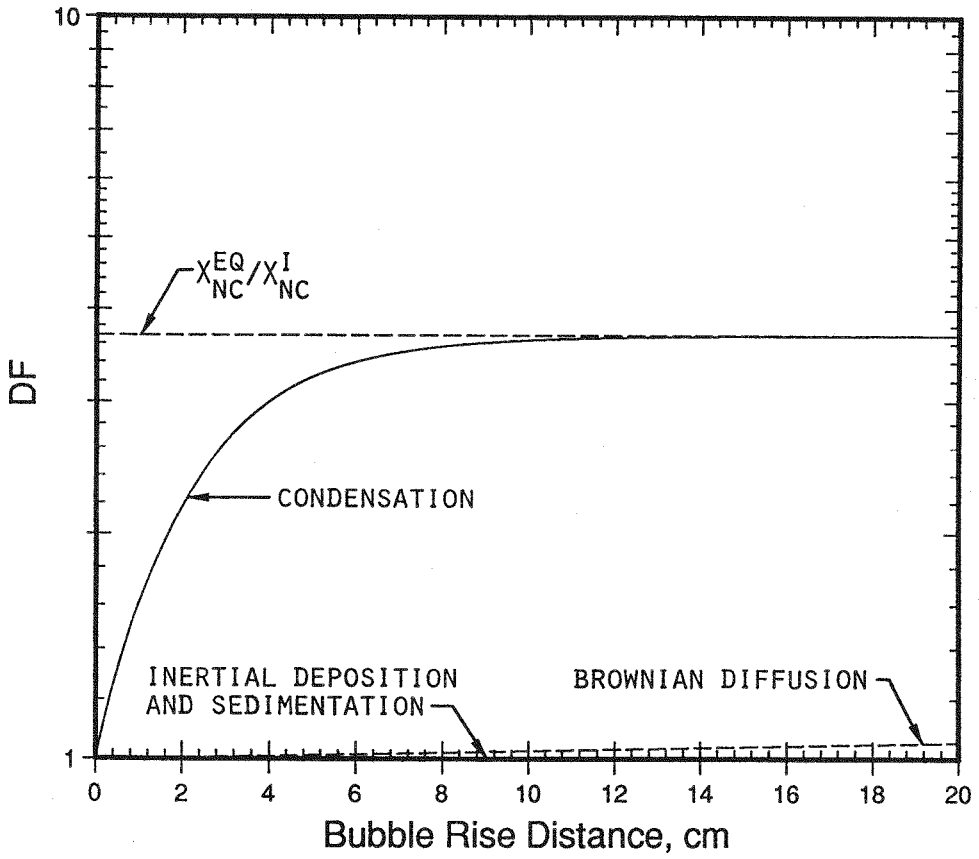

Fig. 5. DF's as a Function of Bubble Rise Distance in the Immediate Vicinity of Injection Point. Reference conditions are defined in Table II.

Note from Fig. 5 that the condensation DF calculated using the detailed transient model merges with the approximate solution defined in Eq. (27) after ~10 cm travel distance. The results of this comparison indicate that for pool depths greater than ~5 bubble diameters, integration of the detailed aerosol transport equations is not required to obtain reasonably accurate solutions for the aerosol DF. The reader should be cautioned that this result has not been checked for conditions other than those shown in Table II. However, in the parametric calculations which follow, this assumption is assumed to hold true, and the aerosol DF is evaluated through Eqs. (27) and (29) through (32). The effect of pool depth on aerosol DF as evaluated with the simplified scrubbing models is shown in Fig. 6. Note from this figure that at the reference depth of 8.2 m, the simplified model predicts a total DF of 35, which agrees within 3% of the value predicted by the detailed model (DF = 36; see discussion above). This fairly minor discrepancy can be attributed to the fact that the simplified model does not account for the effect of hydrostatic pressure variation as the bubble ascends through the pool.

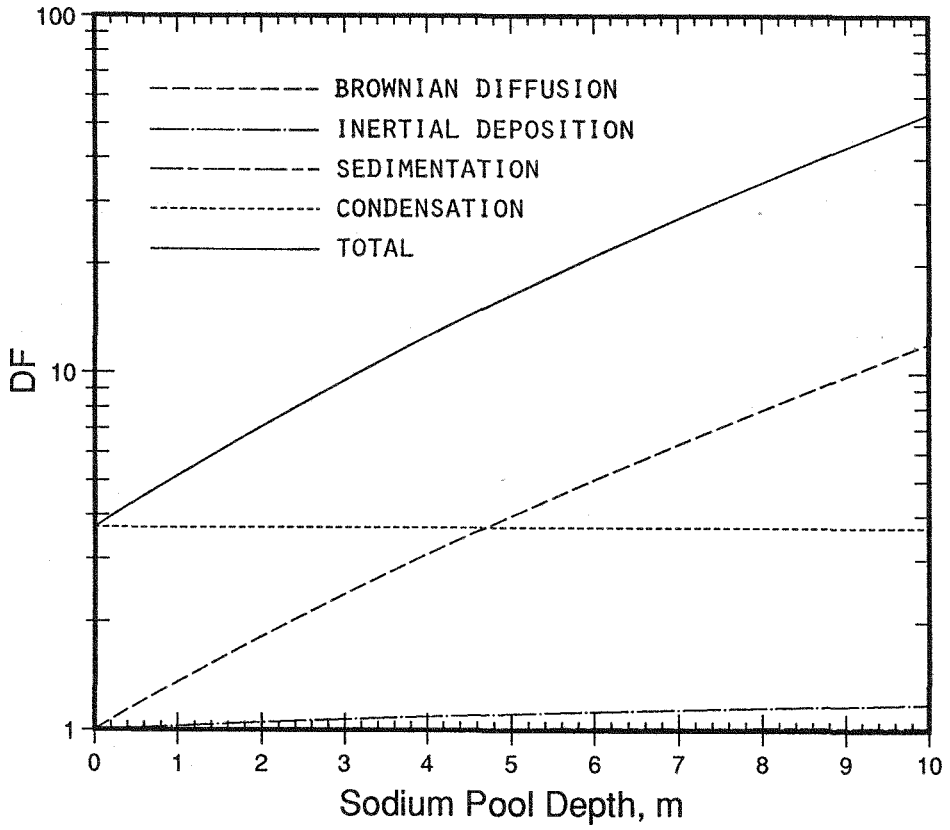

Fig. 6. The Effect of Sodium Pool Depth on DF. Reference conditions are defined in Table II.

The effect of sodium pool temperature on aerosol DF is shown in Fig. 7. Note that over the temperature range 770-970 K, the condensation DF is insensitive to pool temperature, since the vapor pressure of sodium is negligible once the bubble has reached thermal equilibrium with the surrounding coolant. Thus, the condensation DF is principally determined by the initial sodium vapor fraction in the gas phase, which is assumed constant for this case. As is evident from Fig. 7, the overall DF is essentially constant over the pool temperature range under consideration. Note from Eq. (9) that for diffusion scrubbing, which dominates for this particular particle size (0.1 μm), the rate constant is predicted to increase with the square root of bubble temperature (viz. coolant temperature after thermal equilibrium is reached) with all other variables held constant. However, this trend is largely offset by the fact that the equilibrium bubble volume increases linearly with coolant temperature [(i.e., the bubble is assumed to obey the ideal gas law; see Eq. (20)]. The net result is that the diffusion DF, and therefore the overall DF, is essentially constant over this coolant temperature range.

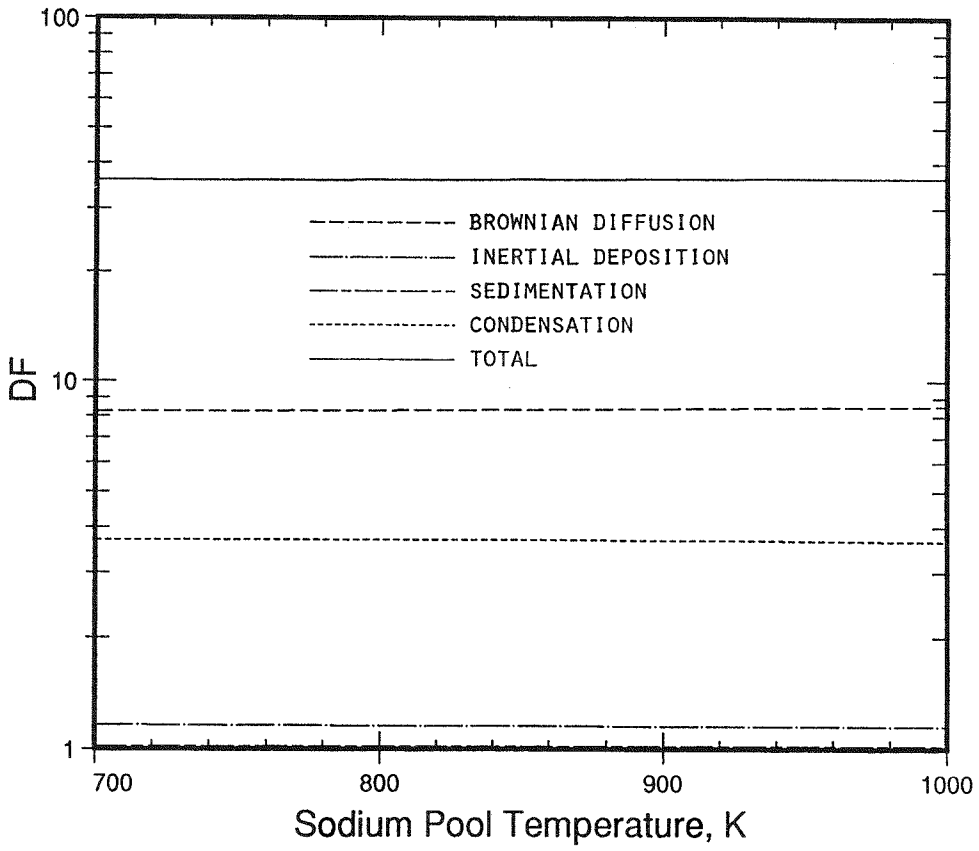

Fig. 7. The Effect of Sodium Pool Temperature on DF. Reference conditions are defined in Table II.

The effect of the initial gas phase sodium vapor content on the aerosol DF is shown in Fig. 8. The condensation DF is noted to increase with increasing vapor content. This trend is due to the fact that the bubble size after reaching thermal equilibrium with the surrounding coolant decreases with increasing vapor content. The fact that the equilibrium bubble size decreases with increasing vapor content also causes increases in the diffusion, inertial deposition, and sedimentation DF's since the rate constants for these processes are all inversely proportional to bubble diameter [see e.g., Eqs. (9), (13,) and (14)]. The net effect of these trends is that the overall aerosol DF rapidly increases with the initial sodium vapor content in the bubble. As is evident from Fig. 8, for vapor contents of >90 mole %, the overall aerosol DF is >1000.

The effect of inlet gas bubble diameter on the aerosol DF is shown in Fig. 9. The diffusion, sedimentation, and inertial deposition DF's are observed to decrease rapidly with increasing bubble diameter. However, the condensation DF is noted to be independent of initial bubble size. This

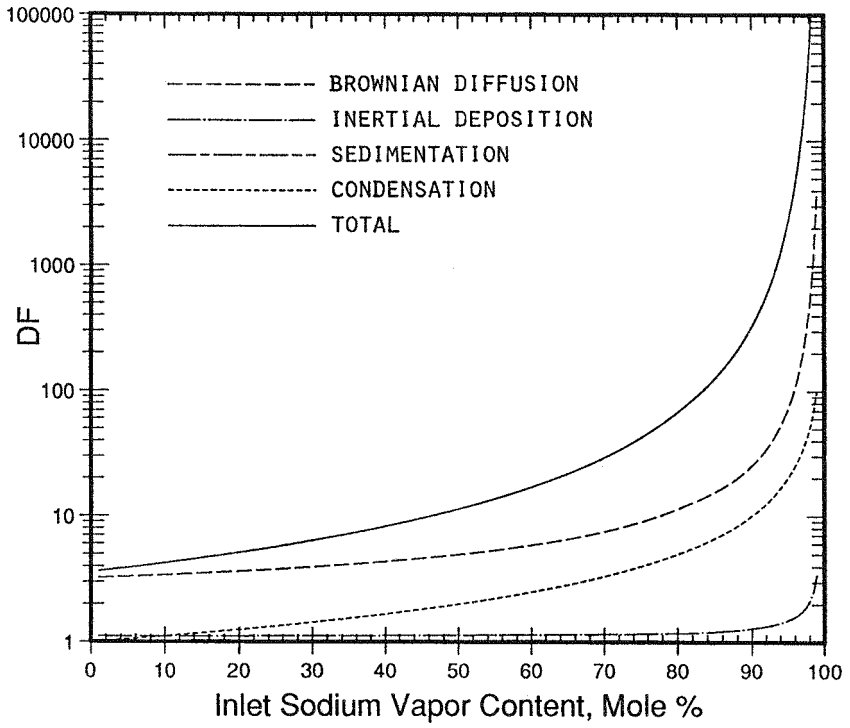

Fig. 8. The Effect of Inlet Sodium Vapor Content on DF. Reference conditions are defined in Table II.

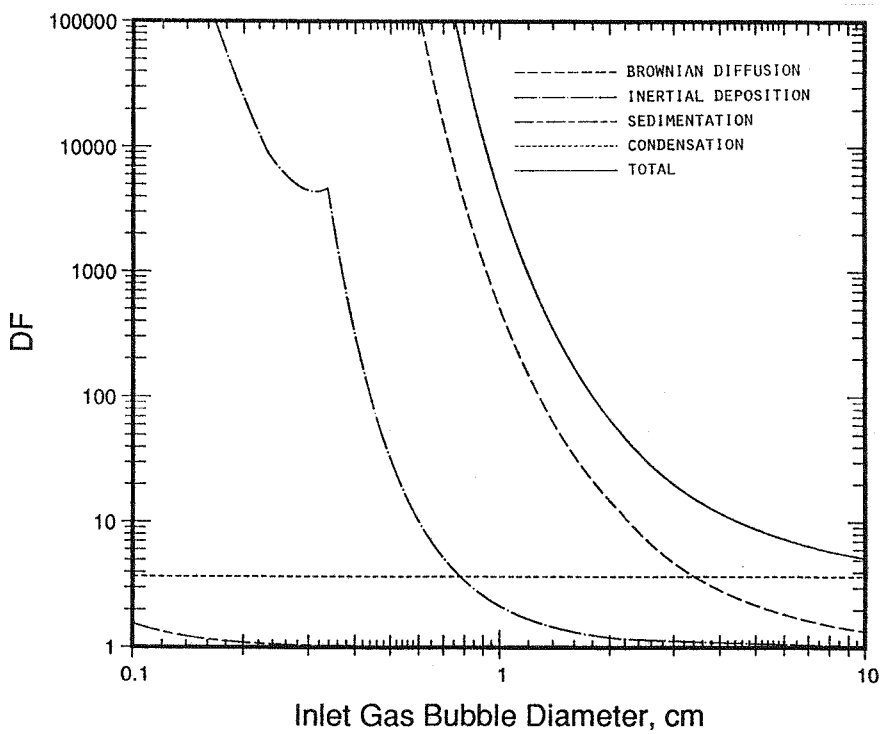

Fig. 9. The Effect of Inlet Gas Bubble Diameter on DF. Reference conditions are defined in Table II.

trend is due to the fact that the degree of condensation is solely determined by the hydrostatic pressure and coolant vapor pressure at the given coolant temperature according to the current model [see Eq. (27)]. The inflection point in the inertial deposition DF near the inlet bubble diameter of 25 mm is due to a peak in the gas bubble rise velocity at this point. The bubble rise velocity [Eq. (36)] and eccentricity [Eq. (39)] as a function of particle diameter are shown in Fig. 10.

The effect of aerosol particle diameter on the overall DF is shown in Fig. 11. As is evident from this figure, the particular scrubbing mechanism which dominates the overall DF is strongly dependent upon the aerosol particle diameter, with the exception of condensation scrubbing, which is independent of particle diameter [see Eq. (27)]. For particles with a diameter of <0.2 μm, diffusion scrubbing dominates. However, the diffusion rate constant is inversely proportional to the square root of the aerosol particle diameter [see Eqs. (4) and (5)], and therefore the diffusion DF decreases with increasing particle diameter. In the particle diameter range of 0.2-0.5 μm, condensation scrubbing dominates the overall DF. For particles with a diameter of >0.5 μm, inertial deposition and sedimentation scrubbing begin to dominate the overall DF, since these two mechanisms are proportional to the particle diameter squared. The net effect of these various competing processes is that a minimum in the overall DF occurs. The minimum occurs in the particle diameter range of 0.2-0.3 μm, where an overall DF of as low as 15 is predicted for the conditions shown in Table II. For particle diameters of <0.06 μm or >1 μm, the overall DF is predicted to be >100.

The results of the parametric calculations regarding aerosol scrubbing in IFR following a core damage event may be summarized as follows. The overall DF for the reference conditions shown in Table II is predicted to be 36. The DF may fall as low as 15 for aerosol particle diameters in the range 0.2-0.3 μm. For particle diameters of <0.06 μm or >1 μm, the DF is predicted to be >100. Factors which strongly influence the DF include the sodium vapor fraction, inlet gas bubble diameter, and aerosol particle diameter. The sodium pool depth plays a significant role in determining the DF, but the inlet gas phase temperature has a negligible effect on the DF.

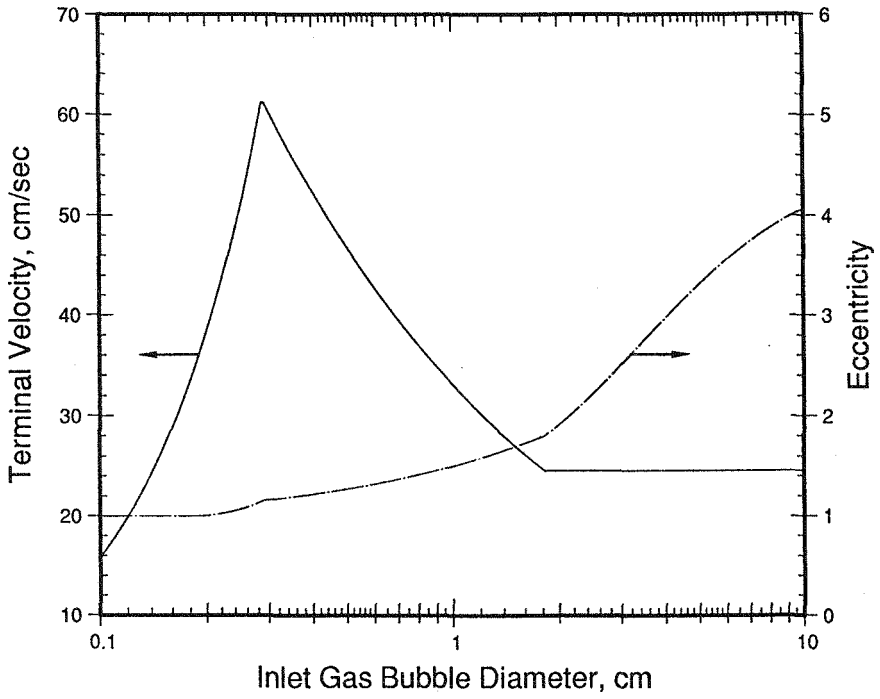

Fig. 10. Terminal Rise Velocity and Eccentricity for Vapor Bubbles in Sodium as a Function of Bubble Diameter. The terminal velocity is calculated with the model of Peebles and Garber,[33] while the bubble eccentricity is calculated with the Tadaki model.

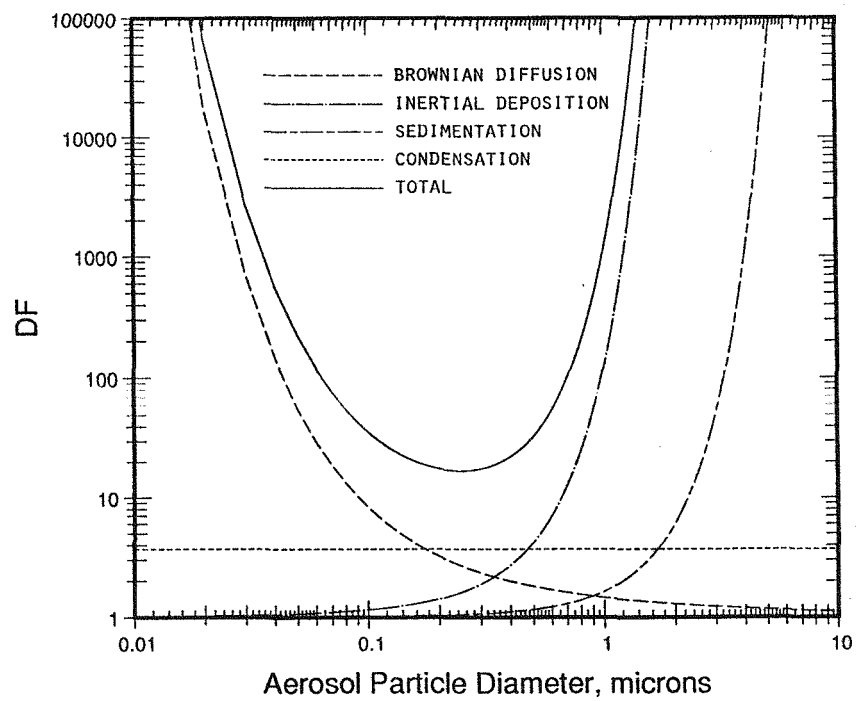

Fig. 11. The Effect of Aerosol Particle Diameter on DF. Reference conditions are defined in Table II.

V. SUMMARY AND CONCLUSIONS

A model has been developed to analyze fission product scrubbing in sodium pools. The modeling approach is to apply classical theories of aerosol scrubbing, developed for the case of isolated bubbles rising through water, to the decontamination of gases produced as a result of postulated core damage event in the liquid metal-cooled IFR. The modeling considers aerosol capture by Brownian diffusion, inertial deposition, and gravitational sedimentation. In addition, the effect of sodium vapor condensation on aerosol scrubbing is treated using both approximate and detailed transient models derived from the literature. The modeling currently does not address thermophoresis or diffusiophoresis scrubbing mechanisms, and is also limited to the scrubbing of discrete aerosol particulate; i.e., the decontamination of volatile gaseous fission products through vapor-phase condensation has not been addressed in this study.

The model has been applied to IFR through a set of parametric calculations focused on determining key modeling uncertainties and sensitivities. Although the design of IFR is not firmly established, representative parameters for the calculations were selected based on the design of the Large Pool Plant (LPP).

The results of the parametric calculations regarding aerosol scrubbing in sodium for conditions relevant to the LPP during a core damage event may be summarized as follows. The overall DF for the reference case (8.2 m pool depth, 770 K pool temperature, 2.4 cm initial bubble diameter, 0.1 μm aerosol particle diameter, 1573 K initial gas phase temperature, and 72.9 mole % initial sodium vapor fraction) is predicted to be 36. The overall DF may fall as low as 15 for aerosol particle diameters in the range 0.2-0.3 μm. For particle diameters of <0.06 μm or >1 μm, the overall DF is predicted to be >100. Factors which strongly influence the overall DF include the inlet sodium vapor fraction, inlet gas bubble diameter, and aerosol particle diameter. The sodium pool depth also plays a significant role in determining the overall DF, but the inlet gas phase temperature has a negligible effect on the DF.

REFERENCES

1. H. P. Planchon, R. M. Singer, D. Mohr, E. E. Feldman, L. K. Chang, and P. R. Betten, "The Experimental Breeder Reactor II Inherent Shutdown and Heat Removal Tests - Results and Analysis," Nucl. Eng. Des., **91**:287 (August 1986).

2. J. E. Cahalan, R. H. Sevy, and S. F. Su, "Accommodation of Unprotected Accidents by Inherent Safety Design Features in Metallic and Oxide-Fueled LMFBR's," Intl. Topical Mtg. on Fast Reactor Safety, **2**:29, Knoxville, TN (April 1985).

3. B. W. Spencer and J. F. Marchaterre, "Scoping Studies of Vapor Behavior During a Severe Accident in a Metal-Fueled Reactor," Intl. Topical Mtg. on Fast Reactor Safety, **2**:151, Knoxville, TN (April 1985).

4. N. A. Fuchs, The Mechanics of Aerosols, Pergamon Press, New York, NY (1964).

5. D. A. Powers, "An Analysis of Radionuclide Behavior in Water Pools During Accidents at the Annular Core Research Reactor," Sandia National Laboratory Report, SAND91-1222 (August 1992).

6. D. A. Powers and J. L. Sprung, "A Simplified Model of Aerosol Scrubbing by a Water Pool Overlying Core Debris Interacting with Concrete," NUREG/CR-5901 (August 1993).

7. L. Talbot, R. D. Cheng, R. W. Sheffer, and D. R. Willis, "Thermophoresis of Particles in a Heated Boundary Layer," J. Fluid Mech., **101**:737 (September 1980).

8. A. T. Wassel, A. F. Mills, and D. C. Bugby, "Analysis of Radionuclide Retention in Water Pools," Nucl. Eng. Des., **90**:87 (May 1985).

9. D. M. Rastler, "Suppression Pool Scrubbing Factors for Postulated Boiling Water Reactor Accident Sequences," General Electric Report, NEDO-25426 (June 1981).

10. S. Guntay, "Experiment Poseidon," Sixth Proc. Nuclear Thermal Hydraulics, **1**:213, Washington, D.C. (November 1990).

11. J. C. Cunnane et al., "The Scrubbing of Fission Product Aerosols in LWR Water Pools Under Severe Accident Conditions-Experimental Results," ANS Topical Mtg. on Fission Product Behavior and Source Term Research, **1**:31-1, Snowbird, UT (July 1984).

12. P. C. Owczarski, R. I. Schreck, and A. K. Postma, "Technical Bases and User's Manual for the Prototype of a Suppression Pool Aerosol Removal Code (SPARC)," NUREG/CR-3317 (May 1985).

13. B. W. Spencer et al., "Results of MACE Tests M0 and M1," Second CSNI Specialist Meeting on Molten Core-Concrete Interactions, Kernforschungszentrum Karlsruhe Report, KfK 5108, 357-373 (April 1992).

14. R. E. Blose et al., "SWISS 1 and 2: Sustained Interaction of Molten Stainless Steel and Concrete in the Presence of Water," NUREG/CR-4727, SAND85-1546, Sandia National Laboratory (July 1987).

15. D. A. Powers, J. E. Brockmann, and A. W. Shiver, "VANESA: A Mechanistic Model of Radionuclide Release and Aerosol Generation During Core Debris Interactions with Concrete," NUREG/CR-4308, SAND85-1370, Sandia National Laboratory (July 1986).

16. P. N. Clough, S. A. Ramsdale, and P. N. Smith, "Aerosol Decontamination Factors in Pools Overlying Molten Core-Concrete - Code Modeling," CSNI Specialists' Meeting on Core-Debris Concrete Interactions, Electric Power Research Institute Report EPRI, NP-5054-SR, 5-49 through 5-60 (February 1987).

17. J. Minges, W. Schütz, and W. Seither, "Investigations on Bubble Behavior and Aerosol Retention in Case of an LMFBR Core Disruptive Accident-the KfK-FAUST Tests," Proc. Intl. Conf. on Fast Reactor Safety, 1:147 London, UK (May 1986).

18. J. C. Petrykowski et al., "Aerosol Release Experiments in the Fuel Aerosol Simulant Test Facility: Undersodium Experiments," NUREG/CR-4346 (September 1985).

19. A. W. Castleman, Jr., "LMFBR Safety, I. Fission-Product Behavior in Sodium," Nucl. Safety, **11**:379 (September 1970).

20. A. E. Klickman and R. C. Callen, "Anomalous Reactivity Effects in the Fermi Incident," Trans. Am. Nuc. Soc., **10**:334 (June 1967).

21. Atomic Power Development Associates, Inc., Power Reactor Development Company, "October 5, 1966, Fuel Damage Incident at the Ennco Fermi Atomic Power Plant, Status as of February 24, 1967," Report NP-16750.

22. R. R. Smith, C. B. Doe, and F. S. Kirn, "The Application of Cover-Gas Monitoring in the Recent EBR-II Fission Product Release," Trans. Am. Nucl. Soc., **10**:634 (November 1967).

23. E. R. Ebersole and R. Villarreal, "Diagnostic Radiochemistry Following the Recent EBR-II Fusion-Product Release," Trans. Am. Nucl. Soc., **10**:634 (November 1967).

24. R. R. Smith et al., "Locating and Identifying the Source of the May 24, 1967, Fission-Product Release in EBR-II," Argonne National Laboratory Report, ANL-7543 (April 1969).

25. M. Epstein, "Theory of Scrubbing of a Volatile Fission Product Vapor-Containing Gas Jet in a Water Pool," ANS Winter Meeting Session on Thermal Hydraulics of Severe Accidents, 1:217, Washington, D.C. (November 1990).

26. R. Jonas and W. Schütz, "Motion and Deposition of Particles in Expanding and Oscillating Gas Bubbles," J. Aerosol Sci., **19**:753 (January 1988).

27. G. I. Taylor, "The Instability of Liquid Surfaces When Accelerated in a Direction Perpendicular to their Plane," Proc. Royal Society, **A201**:192 (January 1950).

28. K. Haga et al., "Equilibrium and Nonequilibrium Partition Coefficients of Volatile Fission Products Between Liquid Sodium and the Gas Phase," Nucl. Tech., **97**:17 (February 1992).

29. S. W. Webb, "Coupling of Aerosol Removal Mechanisms in Rising Bubbles," Trans. Am. Nucl. Soc., **52**:525 (June 1986).

30. T. K. Sherwood, R. L. Pigford, and C. R. Wilke, Mass Transfer, McGraw-Hill, Inc., New York, NY (1975).

31. E. Kreyszig, Advanced Engineering Mathematics, Wiley and Sons, Inc., New York, NY (1972).

32. F. M. White, Viscous Fluid Flow, Appendix C, McGraw-Hill, Inc., New York, NY (1974).

33. F. N. Peebles and H. J. Garber, "Study on the Motion of Gas Bubbles in Liquids," Chem. Eng. Prog., **44**:88 (March 1953).

34. R. Kronig and J. C. Brink, "On the Theory of Extraction from Falling Droplets," Appl. Sci. Res. A, **2**:142 (July 1950).

35. T. C. Huang and J. C. McDonald, "Turbulence Characteristics and Mass Transfer at Air-Water Surfaces ," General Electric Report, GEFR 14034-12 (June 1981).

36. R. B. Bird, W. E. Stewart, and E. N. Lightfoot, Transport Phenomena, John Wiley & Sons, Inc., New York, NY (1960).

37. Ibid., p. 505.

38. L. W. Florscheutz and B. T. Chao, "On the Mechanics of Vapor Bubble Collapse," J. Heat Transfer, **87**:209 (May 1965).

39. H. K. Forster and N. Zuber, "Growth of a Vapor Bubble in a Superheated Liquid," J. Applied Physics, **25**:474 (April 1956).

40. R. C. Weast and M. J. Astle, Eds., CRC Handbook of Chemistry and Physics, CRC Press, Boca Raton, FL (1980).

41. J. K. Fink and L. Leibowitz, "Thermodynamic and Transport Properties of Sodium Liquid and Vapor," Argonne National Laboratory Report, ANL/RE/95/2 (February 1995).